ACS APPLIED MATERIALS & INTERFACES

Research Article

www.acsami.org

Highly Efficient $Ag_2O/Bi_2O_2CO_3$ p-n Heterojunction Photocatalysts with Improved Visible-Light Responsive Activity

Na Liang,[†] Min Wang,[†] Lun Jin,[‡] Shoushuang Huang,[†] Wenlong Chen,[†] Miao Xu,[†] Qingquan He,[†] Jiantao Zai,*[,†] Nenghu Fang,[†] and Xuefeng Qian*[,†]

[†]School of Chemistry and Chemical Engineering and State Key Laboratory of Metal Matrix Composites, Shanghai Jiao Tong University, Shanghai 200240, P. R. China

[‡]Department of Chemistry, University of Warwick, Gibbet Hill, Coventry CV4 7AL, United Kingdom

Supporting Information

ABSTRACT: $Ag_2O/Bi_2O_2CO_3$ p-n heterojunctions are prepared with commercial $Bi_2O_2CO_3$ as precursor via a simple photosynthesis process. The obtained $Ag_2O/Bi_2O_2CO_3$ p-n heterojunctions show higher photocatalytic activity than that of pure n-$Bi_2O_2CO_3$, and the obtained $Ag_2O/Bi_2O_2CO_3$ (AB-4) heterojunction exhibits the best photocatalytic activity under visible light (λ > 400 nm), with which Rhodamine B, methyl blue and methyl orange can be completely degraded within 12 min. Photoluminescent spectra and photoelectrochemical measurement further indicate that the $Ag_2O/Bi_2O_2CO_3$ p-n heterojunctions greatly enhance the charge generation and suppress the charge recombination of photogenerated electron−hole pairs, which would be beneficial to improve their photocatalytic activity.

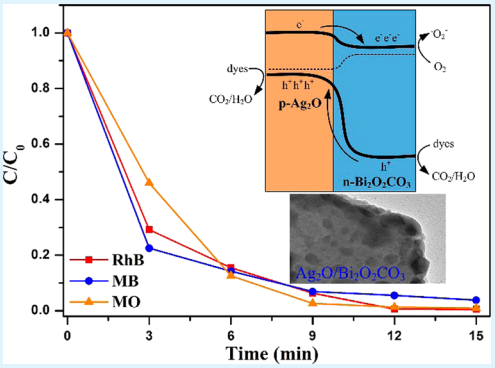

KEYWORDS: *$Bi_2O_2CO_3$, Ag_2O, $Ag_2O/Bi_2O_2CO_3$, photocatalytic activity, p-n heterojunctions, visible light*

1. INTRODUCTION

Because of the shortage of clean water sources and demand for environmental protection, photocatalytic technology has attracted much attention recently.[1−3] Semiconductor photocatalysts, which can effectively absorb and utilize solar energy, have been proven to be available and promising materials for environmental purification.[4,5] Up to now, many semiconductor photocatalysts have been developed for the decomposition of toxic and hazardous organic pollutants, such as TiO_2,[6] $BiVO_4$,[7,8] ZnO,[9,10] $Bi_2O_2CO_3$,[11−13] Bi_2CuO_4,[14] BiOCl,[15,16] and so on. Among these developed photocatalysts, it is vital to find that bismuth subcarbonate ($Bi_2O_2CO_3$) is one of the most attractive photocatalysts for the degradation of organic dyes due to its band gap from 2.87 to 3.5 eV[12] and low mammalian toxicity for medicine treatment.[17] However, common $Bi_2O_2CO_3$ photocatalysts solely absorb UV light due to their wide band gap, which greatly limits their practical applications.[18,19] On the other hand, the photocatalytic efficiency of photocatalysts is also usually limited by the ability of separation and/or combination of photogenerated electron−hole pairs. Therefore, it is necessary to develop an effective strategy to improve charge separation efficiency and enhance visible light responsive activity of photocatalysts.

To improve the photocatalytic activity of $Bi_2O_2CO_3$, some efforts have been recently made, including doping element (N[11,20] and graphene[21]), deposition of metal (Ag[22]) and formation of heterostructures (BiOI,[23] Bi_2MoO_6,[24] $BiVO_4$,[25] etc.). In recent years, fabricating heterojunction in photocatalysts is one of the most ingenious approaches to improve the visible light responsive activity and facilitate the separation of photogenerated electron−hole pairs.[26] For example, n-n heterostructured $Bi_2O_2CO_3/Bi_2WO_6$ nanosheets have been prepared through hydrothermal process and exhibited a good visible light photocatalytic activity toward the degradation of RhB (about 90 min).[27] Similar result has also been found in the $BiVO_4/Bi_2O_2CO_3$ n-n heterostructures with enhanced photocatalytic degradation activity on RhB (around 60 min).[25] Compared with the n-n heterojunctions, p-n heterjunctions have the faster transmission of photogenerated holes, and facilitate the separation of photogenerated electron−hole pairs in photocatalysts, which are quite important for enhancing the photocatalytic activity of photocatalysts.[26,28] Recent works indicated that p-n heterostructured $Fe_3O_4/Bi_2O_2CO_3$ photocatalyst, synthesized by a two-step method, could completely degrade MB and MO within 40 min.[29] Therefore, it is necessary to develop a general and convenient way to prepare these n-n or p-n heterojunction photocatalysts. More recently, we have prepared n-n heterostructured $Bi_2S_3/Bi_2O_2CO_3$ photocatalysts with commercial $Bi_2O_2CO_3$ as precursor, and their enhancing photocatalytic performances and mechanism were carefully studied.[30] However, the obtained n-n heterostructured $Bi_2S_3/Bi_2O_2CO_3$ photocatalysts do not exhibit good

Received: April 23, 2014
Accepted: June 24, 2014
Published: June 24, 2014

chemical and physical stability because the photocorrosion of metal sulfide (Bi_2S_3).[31] Ag_2O is a kind of p-type semiconductors with a direct band gap of 1.46 eV, closing to the ideal value required for photoelectrochemical applications depending on the charge carrier-transfer mechanism.[32] On the other hand, Ag_2O is also suitable to form heterojunction because of its high efficiency, controllability, and facile synthesis processes. Recently, Ag_2O-modificatory TiO_2 has been prepared and displayed a high photocatalytic activity in the decomposition of MO (25 min),[33] also implying the excellent sensitivity of Ag_2O. Thus, it is expected to improve the photocatalytic activity of $Bi_2O_2CO_3$ by fabricating $Ag_2O/Bi_2O_2CO_3$ p-n heterojunction photocatalysts, promoting an interfacial electron transfer process and reducing the charge recombination on semiconductor as a result of the movement of photogenerated electrons to the conduction band of n-type $Bi_2O_2CO_3$[30] and photogenerated holes to the valence band of p-type Ag_2O.

In the present work, $Ag_2O/Bi_2O_2CO_3$ p-n heterojunction photocatalysts are prepared with commercial $Bi_2O_2CO_3$ as precursor via a simple photosynthesis process. The photocatalytic activities of the $Ag_2O/Bi_2O_2CO_3$ heterojunction photocatalysts are evaluated by degrading Rhodamine B (RhB), methyl blue (MB) and methyl orange (MO) under visible-light irradiation. Furthermore, a photocatalytic enhancement mechanism has been proposed based on the relative band gap position of these semiconductors and the integrated heterostructure.

2. EXPERIMENTAL SECTION

Materials. All Chemical reagents of analytic grade purity were purchased from Shanghai Chemical Co. Ltd., and they were directly used without further purification.

Catalysts Synthesis. All samples were synthesized via a simple photosynthesis method. In a typical process, 1.5 mmol of commercial $Bi_2O_2CO_3$ was added to $AgNO_3$ aqueous solution (50 mL) and stirred for 1 h at room temperature. Then the mixed solution was irradiated for 30 min by a 300 W Xe arc lamp under magnetic stirring. After illumination, the suspension was washed with distilled water and dried at 60 °C for 4 h. By controlling the amount of $AgNO_3$ to be 0.250, 0.375, 0.750, 1.500, and 3.000 mmol, the obtained $Ag_2O/Bi_2O_2CO_3$ p-n heterojunction photocatalysts were labeled as AB-1 to AB-5, respectively. Pure Ag_2O samples were synthesized from $AgNO_3$ and NaOH aqueous solution in pH 14.[33,34]

Characterization. Crystallographic structures of samples were investigated by X-ray diffraction (XRD, Shimadzu XRD-6000, Cu−Kα, 40 kV, 30 mA) at a scanning rate of 6° min^{-1}. Energy dispersive X-ray (EDX) spectroscopy was carried on a FEISirion200 scanning electron microscope. Morphology of samples was characterized by transmission electron microscopy (TEM, JEOL, JEM-2100F, 200 kV) and field-emission scanning electron microscopy (FE-SEM; JEOL, JSM-6700F, 5 kV), respectively. X-ray photoelectron spectroscopy (XPS, Versa Probe PHI-5000, ULVAC- PHI Inc.) was used to probe the composition of the obtained samples.UV−vis absorption spectra were recorded on a UV-4100 (Shimadzu) spectrophotometer with $BaSO_4$ as the background between 200 and 2000 nm. Solid-state photoluminescent (PL) spectra were recorded on a Varian Cary-Eclipse 500.

Photocatalytic Activity Test. RhB, MB, and MO were used as model pollutants to evaluate the photocatalytic activity of the obtained $Ag_2O/Bi_2O_2CO_3$ heterojunction photocatalysts. Photodegradation studies of the organic dyes were carried out under a 300 W Xe lamp with a UV-cut filter (λ > 400 nm). $Ag_2O/Bi_2O_2CO_3$ heterojunction photocatalysts (50 mg) were added into 50 mL of RhB, MB, and MO aqueous solution (1.0×10^{-5} M), respectively. The suspensions were sonicated for 5 min and then kept in the dark for 30 min with magnetically stirring to reach an adsorption−desorption equilibrium between photocatalysts and the organic dyes. At a given time interval, 2 mL of sample was taken from the suspension and immediately centrifuged at 4200 rpm for 15 min. Then UV−vis spectra of the centrifuged solution were recorded using a UV-4100 spectrophotometer. The photocatalytic performances of the obtained $Ag_2O/Bi_2O_2CO_3$ heterojunction photocatalysts with different Ag_2O content were also determined to compare the degradation activity of RhB.

Photoelectrochemical Characterization. To prepare working electrodes for the transient photocurrent responses, FTO glass were ultrasonically cleaned in soap-suds, deionized water and acetone, respectively. The electrodes were prepared by mixing a slurry containing 80% as-prepared photocatalyst, 10% acetylene black and 10% polymer binder (polyvinylidenedifluoride) on FTO glass and then dried in a vacuum oven at 60 °C for 12 h. The area of electrodes is controlled to be 0.6 × 0.6 cm^2. A 300 W Xe lamp was used as light source with a UV-cut filter (λ > 400 nm). Amperometric-I-T curve was recorded on Zennium Workstation (ZAHNER-Elektrik GmbH &Co.KG, Germany) in a three-electrode system with Pt mesh as counter electrode, saturated calomel electrode as reference electrode, and 0.5 M Na_2SO_4 aquous solution.

3. RESULTS AND DISCUSSION

Theoretical Band Structure of $Ag_2O/Bi_2O_2CO_3$ p-n Heterojunctions. Theoretical band structure of $Ag_2O/Bi_2O_2CO_3$ p-n heterojunction is constructed to evaluate the effects of structure on their properties. First, the band gaps of commercial $Bi_2O_2CO_3$ and Ag_2O (synthesized by a chemical method) are characterized (vide infra), and the band positions of Ag_2O and $Bi_2O_2CO_3$ can be predicted by the following eqs 1 and 2, respectively.[35]

$$E_{VB} = X - E^e + 0.5E_g \quad (1)$$

$$E_{CB} = E_{VB} - E_g \quad (2)$$

where E_g is the band gap energy of semiconductor; E_{VB} is valence band (VB) edge potentials; E_{CB} is conduction band (CB) edge potentials; X is the electronegativity of semiconductor, which is the geometric mean of the electronegativity of constituent atoms (X_{Bi} = 4.69 eV, X_{Ag} = 4.44 eV, X_O = 7.54 eV, X_C = 6.27 eV[36]); E^e is the energy of free electrons on hydrogen scale (4.5 eV). The values of calculated X, E_{VB}, E_{CB}, and E_g are listed in Table 1.

Table 1. Values of Calculated X, E_{VB}, E_{CB}, and E_g for Ag_2O and $Bi_2O_2CO_3$

semiconductor	electronegativity (eV)	E_{VB} (eV)	E_{CB} (eV)	E_g (eV)
Ag_2O	5.29	1.44	0.14	1.30
$Bi_2O_2CO_3$	6.54	3.66	0.42	3.24

Based on the data listed in Table 1, the theoretical band structure of $Ag_2O/Bi_2O_2CO_3$ heterojunctions can be proposed. From the flatband potentials[37] of valence and conduction band positions at pH 7 for p-Ag_2O and n-$Bi_2O_2CO_3$ with their band gap energy, it is obvious that p-Ag_2O and n-$Bi_2O_2CO_3$ semiconductor are conducive to form heterojunction due to their suitable band gap and energy band positions (see Scheme S1a in the Supporting Information). Fermi level (dotted line) is the chemical potential of thermodynamic equilibrium, p-Ag_2O and n-$Bi_2O_2CO_3$ semiconductors normally have different positions of the Fermi levels when they are separated or pre-equilibrium (see Scheme S1a in the Supporting Information).[38−40] When p-Ag_2O and n-$Bi_2O_2CO_3$ semiconductors

form p-n heterojunction in dark, electrons (e^-) will move from the CB of n-$Bi_2O_2CO_3$ to p-Ag_2O because of the higher Fermi level of n type semiconductor, and the holes (h^+) flow in an opposite direction (see Scheme S1b in the Supporting Information). The flowing of charge carriers (electrons and holes) can generate a depletion layer (positively charged region) in the $Bi_2O_2CO_3$ side, and an accumulation layer (negatively charged region) in the Ag_2O side of Ag_2O/$Bi_2O_2CO_3$ heterojuction. Finally, the depletion and accumulation layers lead to a built-in potential from $Bi_2O_2CO_3$ to Ag_2O. After the charge equilibrium being built, both Ag_2O and $Bi_2O_2CO_3$ semiconductors have the same Fermi level. In other words, they have same chemical potential. So no degradation will happen in dark.

However, when they are exposed to solar illumination, the photogenerated carriers will break the thermodynamic equilibrium, and generate quasi-Fermi levels (quasi-static equilibrium) for each semiconductor (Scheme 1 and Figure S1c in the Supporting Information). Because of the built-in potential in the Ag_2O/$Bi_2O_2CO_3$ p-n heterojuctions, the photogenerated electrons in the accumulation layer of Ag_2O side will drift to the depletion layer of $Bi_2O_2CO_3$ side, and result in the anodic shift of quasi-Fermi level of $Bi_2O_2CO_3$, whereas the drifting of photogenerated holes lead to the cathodic shift of quasi-Fermi level of Ag_2O. The holes can be consumed to oxidize OH^- to form ·OH or directly oxidize dyes. Meanwhile, electrons can reduce the surface chemisorbed O_2 to produce the strong oxidizing species $O_2^{-\bullet}$, which can break down the chromophores of dyes into small molecules, e.g., H_2O and CO_2.[41−43] Finally, quasi-equilbrium energy band structure of p-n heterojunction would be formed under solar illumination. Therefore, the photogenerated carriers can be efficiently separated and the photogenerated holes (electrons) will be concentrated on the Ag_2O ($Bi_2O_2CO_3$) and consumed. So the photocatalytic efficiency of Ag_2O/$Bi_2O_2CO_3$ p-n heterojuctions would be improved compared with Bi_2S_3/$Bi_2O_2CO_3$[30] n-n heterojuctions for degradation of RhB under visible irradiation, in which the photogenerated electrons in the accumulation layer of $Bi_2O_2CO_3$ side and holes in the depletion layer of Bi_2S_3 side will drift to the interface of heterojunction and recombine with each other. So we believe that the Ag_2O/$Bi_2O_2CO_3$ p-n heterojunction photocatalysts would be beneficial for the separation of the photogenerated electron−hole pairs than that of n-n heterojunction photocatalysts, which would further improve the photocatalytic activity in the degradation of organic pollution. In addition, because photogenerated electrons preferably drift to the $Bi_2O_2CO_3$ side, Ag_2O in Ag_2O/$Bi_2O_2CO_3$ p-n heterojuctions may avoid being photoreduced to Ag and lead to better stability under visible illumination.

Scheme 1. Theoretical Band Structure of Ag_2O/$Bi_2O_2CO_3$ p-n Heterojunction (quasi-equilibrium under solar illumination)

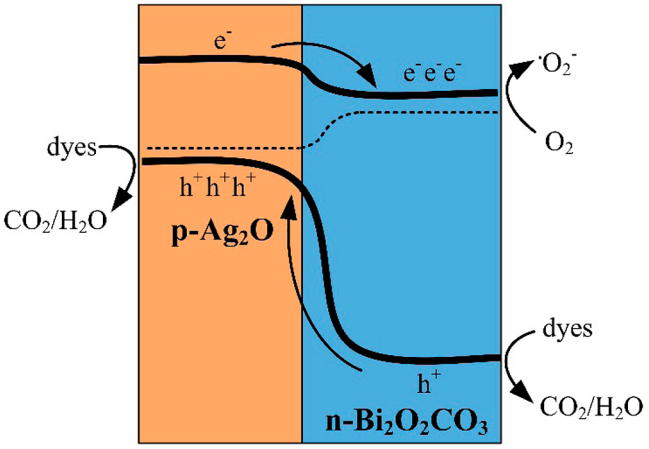

Material Synthesis and Characterization. Ag_2O/$Bi_2O_2CO_3$ heterojunctions are prepared with commercial $Bi_2O_2CO_3$ as precursor via a simple photosynthesis process. Figure 1 shows the XRD patterns of the obtained products and

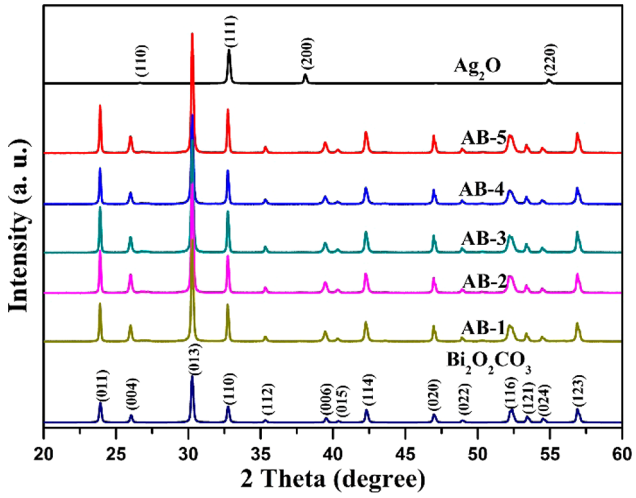

Figure 1. XRD patterns of pure $Bi_2O_2CO_3$, Ag_2O, and the as-prepared Ag_2O/$Bi_2O_2CO_3$ heterojunctions with different $AgNO_3$ content.

the standard patterns of Ag_2O and $Bi_2O_2CO_3$. It indicateds that the diffraction peaks can be assigned to the tetragonal phase of $Bi_2O_2CO_3$ (JCPDS card No. 41−1488, $a = b = 3.87$ Å, $c = 13.67$ Å). The significantly intensified (013) diffraction peaks of Ag_2O/$Bi_2O_2CO_3$ reveal the preferential orientation of (013) crystallographic plane and higher crystallinity of $Bi_2O_2CO_3$. However, no peaks of Ag_2O can be detected even for the AB-4 sample of Ag_2O/$Bi_2O_2CO_3$, because of low content of Ag_2O and high diffraction intensity of $Bi_2O_2CO_3$ to cover the peaks of Ag_2O. Similar phenomenon also appeared in the case of Bi_2S_3/$Bi_2O_2CO_3$,[30] Bi_2S_3/BiOCl[44] and Ag_2O/TiO_2[38] composites. Figure 2 displays the EDX spectroscopy (Figure 2a), cross-sectional SEM (Figure 2b), and elemental mapping images (Figure 2c−f) of the obtained Ag_2O/$Bi_2O_2CO_3$ (AB-4). From which, one can see that Ag element is evenly distributed on the obtained Ag_2O/$Bi_2O_2CO_3$ heterojunction, and SEM images of $Bi_2O_2CO_3$ and Ag_2O/$Bi_2O_2CO_3$ heterojunction reveal that Ag_2O have no obvious effect on the morphology of heterojunctions (see Figures S1 and S2 in the Supporting Information).

The composition and surface electron state of the obtained samples were confirmed by X-ray photoelectron spectroscopy (XPS). Figure 3 shows the XPS spectra of pure $Bi_2O_2CO_3$ and Ag_2O/$Bi_2O_2CO_3$ heterojunction (AB-4). The peaks of Ag 3p and Ag 4d of Ag_2O[33] can be detected in AB-4 sample (marked by the pink dot, Figure 3a). The high-resolution XPS spectra of Bi 4f, C 1s, O 1s, and Ag 3d for the obtained photocatalysts are shown in Figure 3b−e. The binding energies of Bi $4f_{5/2}$ and Bi $4f_{7/2}$ are 164.22 eV/164.19 and 158.93 eV/158.90 eV in AB-4

dx.doi.org/10.1021/am502481z | ACS Appl. Mater. Interfaces 2014, 6, 11698−11705

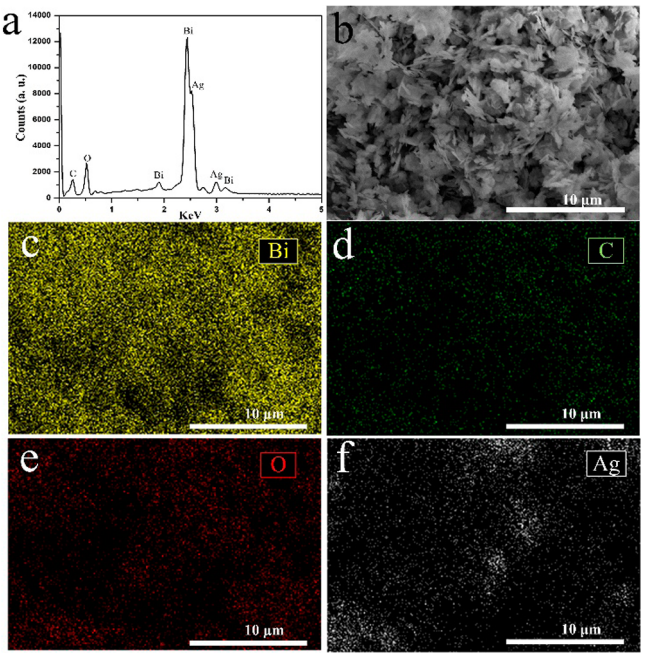

Figure 2. (a) EDX spectra; (b) cross-sectional SEM and elemental distribution maps for (c) Bi, (d) C, (e) O, and (f) Ag of the as-prepared $Ag_2O/Bi_2O_2CO_3$ heterojunction (AB-4).

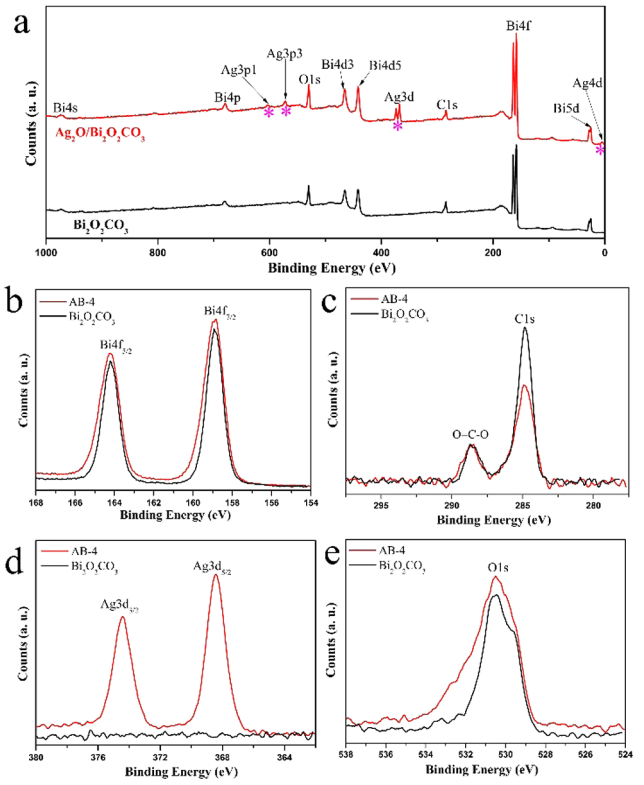

Figure 3. XPS spectra of pure $Bi_2O_2CO_3$ and the as-prepared $Ag_2O/Bi_2O_2CO_3$ heterojunction (AB-4): (a) survey spectra; (b) Bi 3d spectra; (c) C 1s spectra; (d) Ag 3d spectra; and (e) O 1s spectra.

and $Bi_2O_2CO_3$, indicating the existence of Bi (III) (Figure 3b).[45] The peaks of C 1s at 284.90 eV/284.87 and 288.57 eV/288.54 eV correspond to AB-4 and $Bi_2O_2CO_3$, matching well with the literature value of the C and O═C−O in $Bi_2O_2CO_3$ (Figure 3c).[21,46] In the AB-4 sample, the peaks at 374.45 and 368.40 eV can be assigned to Ag $3d_{3/2}$ and Ag $3d_{5/2}$, which are not detected in pure $Bi_2O_2CO_3$ (Figure 3d). And these peaks are consistent with the previous report for Ag_2O.[47] The peaks of O 1s located at 530.56 eV/530.58 eV are ascribed to O in $Bi_2O_2CO_3$ (Figure 3e). The high-resolution O 1s spectrum of AB-4 sample shows a clearly shoulder peak compared with pure $Bi_2O_2CO_3$, indicating the formation of Ag_2O (Figure 3e). The spectra of O 1s can be fitted into three Gaussian-Lorenzian peaks (see Figure S3 in the Supporting Information). The peak located at 529.50 eV is ascribed to O in Bi−O, and the peaks at 532.09 and 530.56 eV can be assigned to the absorbed hydroxyl and carbonate in $Bi_2O_2CO_3$ (see Figure S3a in the Supporting Information).[20,47] For the as-prepared AB-4 (see Figure S3b in the Supporting Information), the binding energy value at 531.39 eV is ascribed to the O in Ag_2O,[47,48] which may cover the low-intensity peaks of hydroxyl. The result also clearly indicates the presence of Ag_2O, implying the formation of $Ag_2O/Bi_2O_2CO_3$ heterojunctions.

Morphology of $Ag_2O/Bi_2O_2CO_3$ Heterojunction Photocatalysts. Figure 4a−c show the TEM images of pure

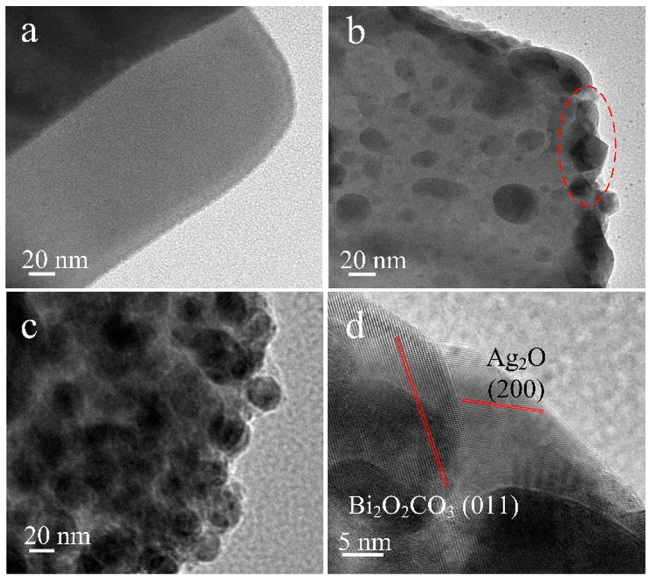

Figure 4. (a) TEM images of $Bi_2O_2CO_3$ and the as-prepared $Ag_2O/Bi_2O_2CO_3$ heterojunctions: (b) AB-4 and (c) AB-5; (d) HRTEM image of AB-4 $Ag_2O/Bi_2O_2CO_3$ heterojunction.

$Bi_2O_2CO_3$ and the as-prepared $Ag_2O/Bi_2O_2CO_3$ heterojunctions with AB-4 and AB-5, respectively. Commercial $Bi_2O_2CO_3$ is in plate-shape morphology, which is in agreement with the previous report (Figure 4a).[30] With the formation of $Ag_2O/Bi_2O_2CO_3$ heterojunctions, numerous Ag_2O nanoparticles appear on the surface of $Bi_2O_2CO_3$ plate and the size of Ag_2O nanoparticles is around 10−50 nm. However, the TEM image of AB-4 (Figure 4b) is very different from that of AB-5 (Figure 4c), in which Ag_2O nanoparticles are much sparse. Figure 4d and Figure S4 in the Supporting Information show the HRTEM image of AB-4 $Ag_2O/Bi_2O_2CO_3$ heterojunction, the clear lattice fringe indicates the coexisting of $Bi_2O_2CO_3$ and Ag_2O, in which the 0.37 nm of lattice spacing is closed to the (011) lattice planes of tetragonal structured $Bi_2O_2CO_3$, while the 0.23 nm of lattice spacing is corresponding to (200) lattice plane of cubic structured Ag_2O. The above results further indicate the formation of heterojunctions between $Bi_2O_2CO_3$ and Ag_2O.

dx.doi.org/10.1021/am502481z | ACS Appl. Mater. Interfaces 2014, 6, 11698−11705

Optical Property of $Ag_2O/Bi_2O_2CO_3$ Heterojunction Photocatalysts. UV–vis absorption spectra of $Bi_2O_2CO_3$, Ag_2O and $Ag_2O/Bi_2O_2CO_3$ heterojunction are shown in Figure 5 and Figure S5a in the Supporting Information. $Bi_2O_2CO_3$ has

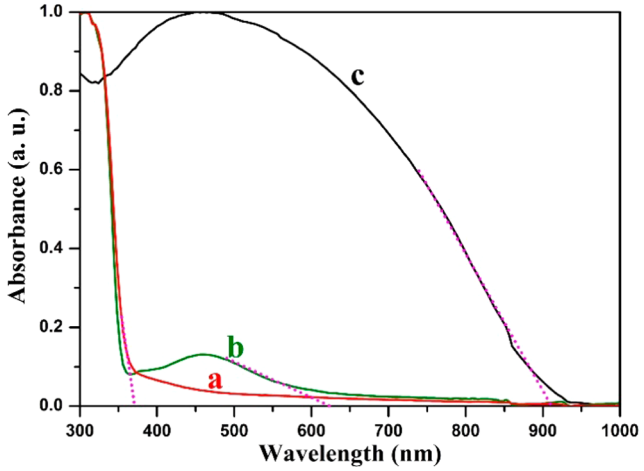

Figure 5. (a) UV–vis absorption spectra of pure $Bi_2O_2CO_3$, (b) $Ag_2O/Bi_2O_2CO_3$ (AB-4) heterojunction and (c) Ag_2O.

a clear edge around 383 nm, and no significant absorbance in visible light region can be seen because of its wide band gap of 3.24 eV (see Figure S5b in the Supporting Information). As for the obtained Ag_2O sample, it exhibits a wide and strong light absorption range of 350–954 nm, and the band gap is determined to be 1.30 eV (see Figure S5c in the Supporting Information). After p-Ag_2O/n-$Bi_2O_2CO_3$ heterojunction being formed, the optical absorption increases in the visible-light region, and the band gap is determined to be around 2.0 eV. Similar phenomena also appeared in the case of Bi_2S_3/CdS/TiO_2 nanotube.[49] It is considered that the energy level will change from quasi-continuous phase to split phase because of the quantum-confinement effect, and the band gap will become wider relative to pure Ag_2O. Thus, $Ag_2O/Bi_2O_2CO_3$ heterojunction has great effects on its optical property and enhances the utilized efficiency of solar light.

Photocatalytic Properties of $Ag_2O/Bi_2O_2CO_3$ Heterojunction Photocatalysts. The photocatalytic activity and chemical stability of $Ag_2O/Bi_2O_2CO_3$ heterojuntion photocatalysts with different Ag_2O content were evaluated by photodegrading the model compounds (RhB, MB and MO) under visible light irradiation. As one can see in Figure 6, the photocatalysis of RhB can be negligible without the presence of $Bi_2O_2CO_3$ or $Ag_2O/Bi_2O_2CO_3$ heterojunction photocatalysts, suggesting that the degradation RhB is induced by photocatalysis. Only approach 20% of RhB can be degraded by pure n-type $Bi_2O_2CO_3$ under visible light irradiation.

In addition, other organic pollutants (MB and MO) were also utilized to evaluate the photocatalytic activity of the obtained $Ag_2O/Bi_2O_2CO_3$ p-n heterojunction photocatalyst (AB-4) with the same molar concentration as that of RhB. As shown in Figure 7, RhB and MO can be completely decomposed and about 95% of MB can be degraded after 12 min under visible light irradiation (λ > 400 nm). Obviously, the degradation ratios of the three dyes almost have no distinction for their different molecular structure.[12] The results further confirm that $Ag_2O/Bi_2O_2CO_3$ p-n heterojunction can be used as a highly efficient visible-light photocatalyst. RhB can be

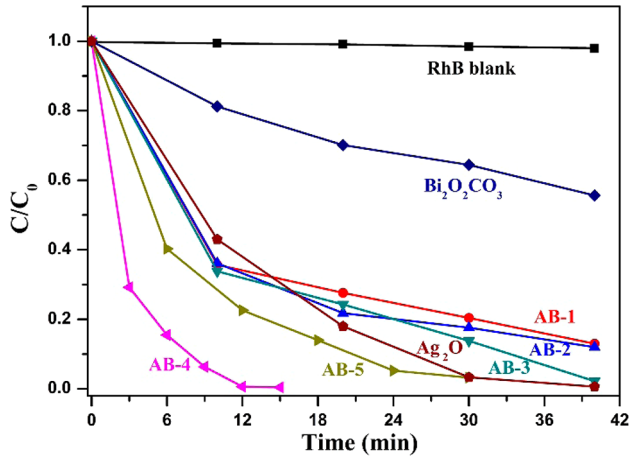

Figure 6. Photocatalytic degradation of RhB with pure $Bi_2O_2CO_3$ and $Ag_2O/Bi_2O_2CO_3$ heterojunctions (with different $AgNO_3$ content) as photocatalysts under visible-light irradiation (λ > 400 nm).

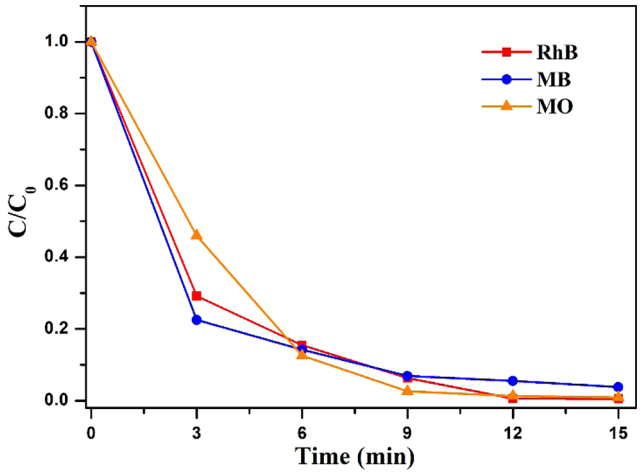

Figure 7. Photocatalytic degradation of RhB, MB, and MO with the as-prepared $Ag_2O/Bi_2O_2CO_3$ heterojunctions (AB-4) as photocatalysts under visible light irradiation (λ > 400 nm).

completely decomposed with the presence of $Ag_2O/Bi_2O_2CO_3$ (AB-4) p-n heterojunction photocatalyst within 12 min under visible light irradiation, which needs much less time than that of n-n heterojuntions based on $Bi_2O_2CO_3$ (usually more than 30 min).[24,30,50] However, further increasing the content of Ag_2O in $Ag_2O/Bi_2O_2CO_3$ heterojunctions, the photocatalytic activity of the obtained $Ag_2O/Bi_2O_2CO_3$ heterojunction photocatalysts decreases, and about 80% of RhB can bedegraded after 12 min for AB-5 heterojunction photocatalyst. The order of photocatalytic activity for $Ag_2O/Bi_2O_2CO_3$ heterojunction photocatalysts can be summarized as following: AB-4> AB-5 > pure Ag_2O > AB-3 > AB-2 > AB-1 > single $Bi_2O_2CO_3$. From which, one can see that the formation of p-n heterojunction is beneficial to improve the photocatalytic activity of as-prepared photocatalysts, the content Ag_2O in the prepared $Ag_2O/Bi_2O_2CO_3$ p-n heterojunction plays important role, and it reaches maximum value of photocatalytic activity at the molar ratio of Ag_2O and $Bi_2O_2CO_3$ presented in AB-4. The photocatalytic activity of the pure Ag_2O particles is better than that of AB-1, AB-2 and AB-3 because of low content of Ag_2O.

From the viewpoint of applications, the chemical and physical stabilities of photocatalysts are significant important during photocatalytic reactions. To further test the photocatalytic performance of the as-prepared $Ag_2O/Bi_2O_2CO_3$ heterojunction photocatalyst (AB-4), recycling experiments were conducted. As shown in Figure 8, the photodegradation

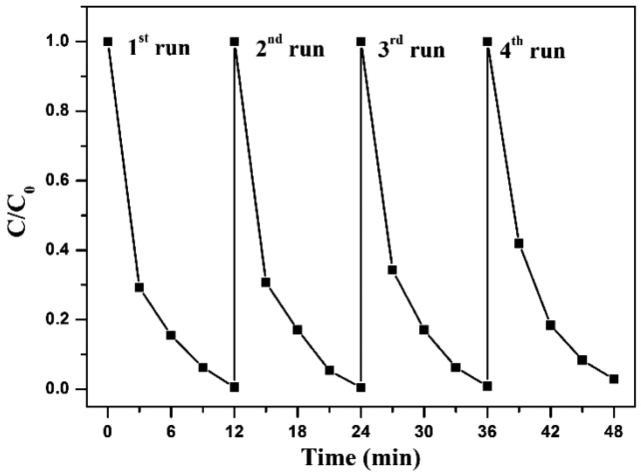

Figure 8. Cycling runs of the as-prepared $Ag_2O/Bi_2O_2CO_3$ heterojunction photocatalyst (AB-4) for degradation of RhB under visible light irradiation (λ > 400 nm).

rate remains similar level after four consecutive cycles, implying that the obtained $Ag_2O/Bi_2O_2CO_3$ heterojuntion photocatalyst has high stability and no photocorrosion happens during the photodegration of RhB. On the other hand, XRD patterns and XPS spectras show that $Ag_2O/Bi_2O_2CO_3$ heterojunction (AB-4) has no obvious differences before and after degradation of RhB (see Figure S6 in the Supporting Information and Figure 8).

Photocatalytic Mechanism. The above results reveal that the as-prepared $Ag_2O/Bi_2O_2CO_3$ p-n heterojunction photocatalysts exhibit higher photocatalytic activity than pure $Bi_2O_2CO_3$ and $Bi_2S_3/Bi_2O_2CO_3$ n-n heterojunctions,[30] as a result of the benefits from their special band structure (Scheme 1), and $Ag_2O/Bi_2O_2CO_3$ heterojunction (AB-4) has the highest photocatalytic activity. To further verified these benefits, photoluminescence (PL) spectra is used to investigate the separation rate of the photogenerated electron−hole pairs because the decrease in the recombination rate gives rise to a low PL intensity.[51] From PL spectra of $Bi_2O_2CO_3$ and $Ag_2O/Bi_2O_2CO_3$ heterojunctions with different content of Ag_2O excited at 220 nm (Figure 9), one can see that the PL intensity around 352 nm gradually decreases with the increase of Ag_2O content in the $Ag_2O/Bi_2O_2CO_3$ heterojunctions, implying p-n heterojunctions can deeply suppress the recombination of electron−hole pairs and lead to lower PL intensity as well as to improve the photocatalytic performances.

On the other hand, photocurrent responses can also provide the evidence for the separation rate of the photogenerated electron−hole pairs in hereojunctions, the transient photocurrent measurements of hereojunctions based photoanodes were investigated. Figure 10 shows the transient curves of electrodes prepared with pure $Bi_2O_2CO_3$, Ag_2O, and the as-prepared $Ag_2O/Bi_2O_2CO_3$ heterojunction (AB-4). Under chopped irradiation of a Xe lamp (λ > 400 nm), both the photocurrent and dark current for $Bi_2O_2CO_3$, Ag_2O, and $Ag_2O/Bi_2O_2CO_3$ heterojunction can reach the equilibrium state immediately, which is also consistent with the previous reports.[39,52] However, the photocurrent of $Ag_2O/Bi_2O_2CO_3$ electrode is much higher than that of $Bi_2O_2CO_3$ and Ag_2O electrode, indicating that $Ag_2O/Bi_2O_2CO_3$ heterojunction has the improved separation of photogenerated electron−hole pairs and can greatly facilitate its photocatalytic activity.

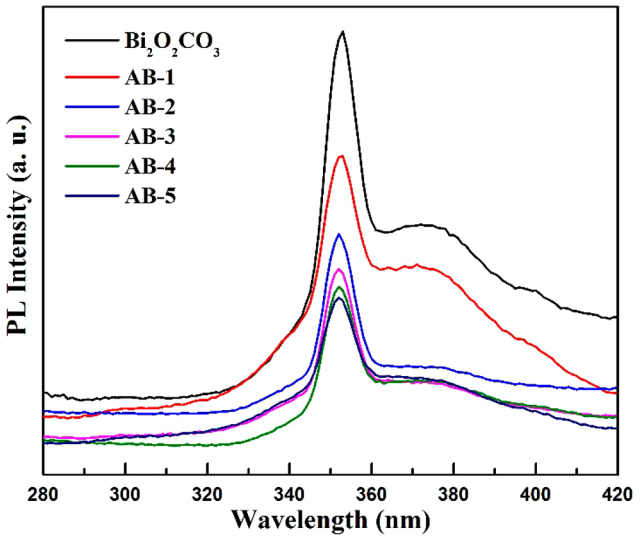

Figure 9. Photoluminescence (PL) spectra of $Bi_2O_2CO_3$ and $Ag_2O/Bi_2O_2CO_3$ heterojunction with different molar ratios.

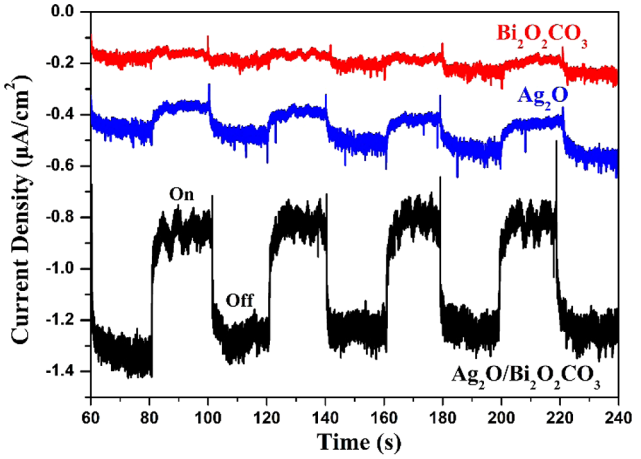

Figure 10. Current−time curves of electrodes made of pure $Bi_2O_2CO_3$, Ag_2O, and $Ag_2O/Bi_2O_2CO_3$ heterojunction (AB-4).

4. CONCLUSIONS

A series of $Ag_2O/Bi_2O_2CO_3$ p-n heterojunctions are successfully fabricated with commercial $Bi_2O_2CO_3$ by a simple photosynthesis method. The photocatalytic activity of the obtained heterojunction photocatalysts is evaluated by degrading RhB, MB and MO under visible light (λ > 400 nm), and these model compounds can be completely degraded within 12 min. The high photocatalytic activity of heterojunction photocatalysts could be attributed to their good visible light absorption and efficient separation of photogenerated electron−hole pairs, which has been supported by the photoluminescent spectra and photoelectrochemical measurement. Furthermore, a photocatalytic enhancement mechanism of the p-n heterojunctions has been proposed based on the

relative band gap position of these two semiconductors and the integrated heterostructure. The work would provide a simple and cheap method to prepare higher effective photocatalysts with more stability, and the convenient and green method can be extended to other bismuth-containing heterostructured photocatalysts with highly efficient photocatalytic performances. Overall, the obtained photocatalysts would have potential applications in future.

■ ASSOCIATED CONTENT

Supporting Information

Theoretical band structure of $Ag_2O/Bi_2O_2CO_3$ p-n heterojunction; (a) SEM images of $Bi_2O_2CO_3$ and (b) $Ag_2O/Bi_2O_2CO_3$ (AB-4) heterojunction; SEM and TEM images of the as-prepared Ag2O/$Bi_2O_2CO_3$ heterojunctions: (a-b) AB-1, (c-d) AB-2 and (e-f) AB-3; O 1s spectra of (a) pure $Bi_2O_2CO_3$ and (b) the as-prepared $Ag_2O/Bi_2O_2CO_3$ heterojunction (AB-4); HRTEM image of $Ag_2O/Bi_2O_2CO_3$ (AB-4) heterojunction; UV−vis absorption spectra of (a) pure $Bi_2O_2CO_3$, $Ag_2O/Bi_2O_2CO_3$ (AB-1, AB-2, AB-3, AB-4, and AB-5) heterojunction and Ag_2O, (b-c) band gap evaluation from the plot of $(ahv)^{1/n}$ vs hv; XRD patterns of $Ag_2O/Bi_2O_2CO_3$ (AB-4) heterojunction before and after photocatalysis; XPS spectra of pure $Bi_2O_2CO_3$ and the as-prepared $Ag_2O/Bi_2O_2CO_3$ heterojunction (AB-4) before and after degradation of RhB: (a) survey spectra; (b) Bi 3d spectra; (c) C 1s spectra; (d) Ag 3d spectra and (e) O 1s spectra. This material is available free of charge via the Internet at http://pubs.acs.org.

■ AUTHOR INFORMATION

Corresponding Authors

*E-mail: xfqian@sjtu.edu.cn. Fax: +86-21-54741297. Tel: +86-21-54743262.

*E-mail: zaijiantao@sjtu.edu.cn.

Notes

The authors declare no competing financial interest.

■ ACKNOWLEDGMENTS

The work was supported by the Program of National Natural Science Foundation of China (21371121 and 21331004), Shanghai Chenguang-Project (13CG10) and Nano-Project (12 nm0504300) and Minhang District Developing Project.

■ REFERENCES

(1) Asahi, R.; Morikawa, T.; Ohwaki, T.; Aoki, K.; Taga, Y. Visible-Light Photocatalysis in Nitrogen-Doped Titanium Oxides. *Science* **2001**, *293*, 269−271.

(2) Chong, M. N.; Jin, B.; Chow, C. W. K.; Saint, C. Recent Developments in Photocatalytic Water Treatment Technology: A Review. *Water Res.* **2010**, *44*, 2997−3027.

(3) Dai, F.; Zai, J.; Yi, R.; Gordin, M. L.; Sohn, H.; Chen, S.; Wang, D. Bottom-up Synthesis of High Surface Area Mesoporous Crystalline Silicon and Evaluation of Its Hydrogen Evolution Performance *Nat. Commun.* **2014**, *5*.

(4) Lei, Z.; You, W.; Liu, M.; Zhou, G.; Takata, T.; Hara, M.; Domen, K.; Li, C. Photocatalytic Water Reduction under Visible Light on a Novel $ZnIn_2S_4$ Catalyst Synthesized by Hydrothermal Method. *Chem. Commun.* **2003**, 2142−2143.

(5) Subramanian, V.; Wolf, E. E.; Kamat, P. V. Catalysis with TiO_2/Gold Nanocomposites. Effect of Metal Particle Size on the Fermi Level Equilibration. *J. Am. Chem. Soc.* **2004**, *126*, 4943−4950.

(6) Xu, H.; Reunchan, P.; Ouyang, S.; Tong, H.; Umezawa, N.; Kako, T.; Ye, J. Anatase TiO_2 Single Crystals Exposed with High-Reactive {111} Facets Toward Efficient H_2 Evolution. *Chem. Mater.* **2013**, *25*, 405−411.

(7) Kim, T. W.; Choi, K.-S. Nanoporous $BiVO_4$ Photoanodes with Dual-Layer Oxygen Evolution Catalysts for Solar Water Splitting. *Science* **2014**, *343*, 990−994.

(8) Zhang, Y.; Li, G.; Yang, X.; Yang, H.; Lu, Z.; Chen, R. Monoclinic $BiVO_4$ Micro-/Nanostructures: Microwave and Ultrasonic Wave Combined Synthesis and Their Visible-Light Photocatalytic Activities. *J. Alloys Compd.* **2013**, *551*, 544−550.

(9) Lin, F.; Cojocaru, B.; Chou, C. L.; Cadigan, C. A.; Ji, Y.; Nordlund, D.; Weng, T. C.; Zheng, Z.; Pârvulescu, V. I.; Richards, R. M. Photocatalytic Activity and Selectivity of ZnO Materials in the Decomposition of Organic Compounds. *ChemCatChem.* **2013**, *5*, 3841−3846.

(10) Fang, J.; Fan, H.; Dong, G. A Facile Way to Synthesize Cost-Effective ZnO Nanorods with Enhanced Photocatalytic Activity. *Mater. Lett.* **2014**, *120*, 147−150.

(11) Dong, F.; Xiong, T.; Zhao, Z.; Sun, Y.; Fu, M. Ammonia Induced Formation of N-Doped $(BiO)_2CO_3$ Hierarchical Microspheres: the Effect of Hydrothermal Temperature on the Morphology and Photocatalytic Activity. *CrystEngComm* **2013**, *15*, 10522−10532.

(12) Zhao, T.; Zai, J.; Xu, M.; Zou, Q.; Su, Y.; Wang, K.; Qian, X. Hierarchical $Bi_2O_2CO_3$ Microspheres with Improved Visible-Light-Driven Photocatalytic Activity. *CrystEngComm* **2011**, *13*, 4010−4017.

(13) Zheng, Y.; Duan, F.; Chen, M.; Xie, Y. Synthetic $Bi_2O_2CO_3$ Nanostructures: Novel Photocatalyst with Controlled Special Surface Exposed. *J. Mol. Catal. A: Chem.* **2010**, *317*, 34−40.

(14) Zhang, Y.; Li, G.; Zhao, H.; Tian, F.; Xiao, S.; Chen, R. Controllable Synthesis of Hierarchical Bi_2CuO_4 Microspheres in Aqueous Solution and Their Highly Efficient Visible-Light-Driven Photocatalytic Activities. *CrystEngComm* **2013**, *15*, 8159−8165.

(15) Zhang, X.; Ai, Z.; Jia, F.; Zhang, L. Generalized One-Pot Synthesis, Characterization, and Photocatalytic Activity of Hierarchical BiOX (X = Cl, Br, I) Nanoplate Microspheres. *J. Phys. Chem. C* **2008**, *112*, 747−753.

(16) Xiong, J.; Cheng, G.; Qin, F.; Wang, R.; Sun, H.; Chen, R. Tunable BiOCl Hierarchical Nanostructures for High-Efficient Photocatalysis under Visible Light Irradiation. *Chem. Eng. J.* **2013**, *220*, 228−236.

(17) Gan, H.; Zhang, G.; Huang, H. Enhanced Visible-Light-Driven Photocatalytic Inactivation of Escherichia Coli by $Bi_2O_2CO_3/Bi_3NbO_7$ Composites. *J. Hazard. Mater.* **2013**, *250−251*, 131−137.

(18) Zhou, W.; Yin, Z.; Du, Y.; Huang, X.; Zeng, Z.; Fan, Z.; Liu, H.; Wang, J.; Zhang, H. Synthesis of Few-Layer MoS_2 Nanosheet-Coated TiO_2 Nanobelt Heterostructures for Enhanced Photocatalytic Activities. *Small* **2013**, *9*, 140−147.

(19) Kowalska, E.; Remita, H.; Colbeau-Justin, C.; Hupka, J.; Belloni, J. Modification of Titanium Dioxide with Platinum Ions and Clusters: Application in Photocatalysis. *J. Phys. Chem. C* **2008**, *112*, 1124−1131.

(20) Dong, F.; Liu, H.; Ho, W.-K.; Fu, M.; Wu, Z. $(NH_4)_2CO_3$ Mediated Hydrothermal Synthesis of N-Doped $(BiO)_2CO_3$ Hollow Nanoplates Microspheres as High-Performance and Durable Visible Light Photocatalyst for Air Cleaning. *Chem. Eng. J.* **2013**, *214*, 198−207.

(21) Madhusudan, P.; Yu, J.; Wang, W.; Cheng, B.; Liu, G. Facile Synthesis of Novel Hierarchical Graphene-$Bi_2O_2CO_3$ Composites with Enhanced Photocatalytic Performance under Visible Light. *Dalton Trans.* **2012**, *41*, 14345−14353.

(22) Peng, S.; Li, L.; Tan, H.; Wu, Y.; Cai, R.; Yu, H.; Huang, X.; Zhu, P.; Ramakrishna, S.; Srinivasan, M.; Yan, Q. Monodispersed Ag Nanoparticles Loaded on the PVP-Assisted Synthetic $Bi_2O_2CO_3$ Microspheres with Enhanced Photocatalytic and Supercapacitive Performances. *J. Mater. Chem. A* **2013**, *1*, 7630−7638.

(23) Cao, J.; Li, X.; Lin, H.; Chen, S.; Fu, X. In Situ Preparation of Novel p−n Junction Photocatalyst BiOI/$(BiO)_2CO_3$ with Enhanced Visible Light Photocatalytic Activity. *J. Hazard. Mater.* **2012**, *239−240*, 316−324.

(24) Xu, Y.-S.; Zhang, W.-D. Anion Exchange Strategy for Construction of Sesame-Biscuit-Like $Bi_2O_2CO_3/Bi_2MoO_6$ Nano-

composites with Enhanced Photocatalytic Activity. *Appl. Catal., B* **2013**, *140−141*, 306−316.
(25) Madhusudan, P.; Ran, J.; Zhang, J.; Yu, J.; Liu, G. Novel Urea Assisted Hydrothermal Synthesis of Hierarchical $BiVO_4/Bi_2O_2CO_3$ Nanocomposites with Enhanced Visible-Light Photocatalytic Activity. *Appl. Catal., B* **2011**, *110*, 286−295.
(26) Ida, S.; Takashiba, A.; Koga, S.; Hagiwara, H.; Ishihara, T. Potential Gradient and Photocatalytic Activity of an Ultrathin p−n Junction Surface Prepared with Two-Dimensional Semiconducting Nanocrystals. *J. Am. Chem. Soc.* **2014**, *136*, 1872−1878.
(27) Xu, Y.-S.; Zhang, Z.-J.; Zhang, W.-D. Inlay of $Bi_2O_2CO_3$ Nanoparticles onto Bi_2WO_6 Nanosheets to Build Heterostructured Photocatalysts. *Dalton Trans.* **2014**, *43*, 3660−3668.
(28) Zhao, W.-W.; Liu, Z.; Shan, S.; Zhang, W.-W.; Wang, J.; Ma, Z.-Y.; Xu, J.-J.; Chen, H.-Y. Bismuthoxyiodide Nanoflakes/Titania Nanotubes Arrayed p-n Heterojunction and Its Application for Photoelectrochemical Bioanalysis *Sci. Rep.* **2014**, *4*.
(29) Zhu, G.; Hojamberdiev, M.; Katsumata, K.-i.; Cai, X.; Matsushita, N.; Okada, K.; Liu, P.; Zhou, J. Heterostructured $Fe_3O_4/Bi_2O_2CO_3$ Photocatalyst: Synthesis, Characterization and Application in Recyclable Photodegradation of Organic Dyes under Visible Light Irradiation. *Mater. Chem. Phys.* **2013**, *142*, 95−105.
(30) Liang, N.; Zai, J.; Xu, M.; Zhu, Q.; Wei, X.; Qian, X. Novel $Bi_2S_3/Bi_2O_2CO_3$ Heterojunction Photocatalysts with Enhanced Visible Light Responsive Activity and Wastewater Treatment. *J. Mater. Chem. A* **2014**, *2*, 4208−4216.
(31) Kudo, A.; Miseki, Y. Heterogeneous Photocatalyst Materials for Water Splitting. *Chem. Soc. Rev.* **2009**, *38*, 253−278.
(32) Lyu, L. M.; Huang, M. H. Investigation of Relative Stability of Different Facets of Ag_2O Nanocrystals through Face-Selective Etching. *J. Phys. Chem. C* **2011**, *115*, 17768−17773.
(33) Zhou, W.; Liu, H.; Wang, J.; Liu, D.; Du, G.; Cui, J. Ag_2O/TiO_2 Nanobelts Heterostructure with Enhanced Ultraviolet and Visible Photocatalytic Activity. *ACS Appl. Mater. Interfaces* **2010**, *2*, 2385−2392.
(34) Xu, L.; Wei, B.; Liu, W.; Zhang, H.; Su, C.; Che, J. Flower-Like ZnO-Ag_2O Composites: Precipitation Synthesis and Photocatalytic Activity. *Nanoscale Res. Lett.* **2013**, *8*, 1−16.
(35) Long, M.; Cai, W.; Cai, J.; Zhou, B.; Chai, X.; Wu, Y. Efficient Photocatalytic Degradation of Phenol over $Co_3O_4/BiVO_4$ Composite under Visible Light Irradiation. *J. Phys. Chem. B* **2006**, *110*, 20211−20216.
(36) Ghosh, D. C.; Chakraborty, T. Gordy's Electrostatic Scale of Electronegativity Revisited. *J. Mol. Struct. Theochem* **2009**, *906*, 87−93.
(37) White, J. R.; Bard, A. J. Electrochemical Investigation of Photocatalysis at Cadmium Sulfide Suspensions in the Presence of Methylviologen. *J. Phys. Chem.* **1985**, *89*, 1947−1954.
(38) Sarkar, D.; Ghosh, C. K.; Mukherjee, S.; Chattopadhyay, K. K. Three Dimensional Ag_2O/TiO_2 Type-II (p−n) Nanoheterojunctions for Superior Photocatalytic Activity. *ACS Appl. Mater. Interfaces* **2012**, *5*, 331−337.
(39) Mayer, M. T.; Du, C.; Wang, D. Hematite/Si Nanowire Dual-Absorber System for Photoelectrochemical Water Splitting at Low Applied Potentials. *J. Am. Chem. Soc.* **2012**, *134*, 12406−12409.
(40) Seger, B.; Pedersen, T.; Laursen, A. B.; Vesborg, P. C. K.; Hansen, O.; Chorkendorff, I. Using TiO_2 as a Conductive Protective Layer for Photocathodic H_2 Evolution. *J. Am. Chem. Soc.* **2013**, *135*, 1057−1064.
(41) Chen, Y.; Huang, R.; Chen, D.; Wang, Y.; Liu, W.; Li, X.; Li, Z. Exploring the Different Photocatalytic Performance for Dye Degradations over Hexagonal $ZnIn_2S_4$ Microspheres and Cubic $ZnIn_2S_4$ Nanoparticles. *ACS Appl. Mater. Interfaces* **2012**, *4*, 2273−2279.
(42) Hu, S.; Zhu, J.; Wu, L.; Wang, X.; Liu, P.; Zhang, Y.; Li, Z. Effect of Fluorination on Photocatalytic Degradation of Rhodamine B over $In(OH)_yS_z$: Promotion or Suppression? *J. Phys. Chem. C* **2010**, *115*, 460−467.
(43) Li, Z.; Dong, H.; Zhang, Y.; Dong, T.; Wang, X.; Li, J.; Fu, X. Effect of M^{2+} (M =Zn and Cu) Dopants on the Electronic Structure and Photocatalytic Activity of $In(OH)_yS_z$ Solid Solution. *J. Phys. Chem. C* **2008**, *112*, 16046−16051.
(44) Cheng, H.; Huang, B.; Qin, X.; Zhang, X.; Dai, Y. A Controlled Anion Exchange Strategy to Synthesize Bi_2S_3 Nanocrystals/BiOCl Hybrid Architectures with Efficient Visible Light Photoactivity. *Chem. Commun.* **2012**, *48*, 97−99.
(45) Li, Q.; Liu, H.; Dong, F.; Fu, M. Hydrothermal Formation of N-Doped $(BiO)_2CO_3$ Honeycomb-Like Microspheres Photocatalysts with Bismuth Citrate and Dicyandiamide as Precursors. *J. Colloid Interface Sci.* **2013**, *408*, 33−42.
(46) Yu, C.; Li, G.; Kumar, S.; Yang, K.; Jin, R. Phase Transformation Synthesis of Novel Ag_2O/Ag_2CO_3 Heterostructures with High Visible Light Efficiency in Photocatalytic Degradation of Pollutants. *Adv. Mater.* **2014**, *26*, 892−898.
(47) Xu, M.; Han, L.; Dong, S. Facile Fabrication of Highly Efficient g-C_3N_4/Ag_2O Heterostructured Photocatalysts with Enhanced Visible-Light Photocatalytic Activity. *ACS Appl. Mater. Interfaces* **2013**, *5*, 12533−12540.
(48) Weaver, J. F.; Hoflund, G. B. Surface Characterization Study of the Thermal Decomposition of Ag_2O. *Chem. Mater.* **1994**, *6*, 1693−1699.
(49) Lv, P.; Fu, W.; Yang, H.; Sun, H.; Chen, Y.; Ma, J.; Zhou, X.; Tian, L.; Zhang, W.; Li, M.; Yao, H.; Wu, D. Simple Synthesis Method of Bi_2S_3/CdS Quantum Dots Cosensitized TiO_2 Nanotubes Array with Enhanced Photoelectrochemical and Photocatalytic Activity. *CrystEngComm* **2013**, *15*, 7548−7555.
(50) Huang, X.; Chen, H. One-Pot Hydrothermal Synthesis of $Bi_2O_2CO_3/Bi_2WO_6$ Visible Light Photocatalyst with Enhanced Photocatalytic Activity. *Appl. Surf. Sci.* **2013**, *284*, 843−848.
(51) Yue, W.; Han, S.; Peng, R.; Shen, W.; Geng, H.; Wu, F.; Tao, S.; Wang, M. $CuInS_2$ Quantum Dots Synthesized by a Solvothermal Route and Their Application as Effective Electron Acceptors for Hybrid Solar Cells. *J. Mater. Chem.* **2010**, *20*, 7570−7578.
(52) Lin, Y.; Xu, Y.; Mayer, M. T.; Simpson, Z. I.; McMahon, G.; Zhou, S.; Wang, D. Growth of p-Type Hematite by Atomic Layer Deposition and Its Utilization for Improved Solar Water Splitting. *J. Am. Chem. Soc.* **2012**, *134*, 5508−5511.